On the Reaction Mechanism of Direct H$_2$O$_2$ Formation over Pd Catalysts

(article starts on next page)

On the Reaction Mechanism of Direct H$_2$O$_2$ Formation over Pd Catalysts

Lin Chen,* J. Will Medlin, and Henrik Grönbeck*

Read Online

ACCESS | Metrics & More | Article Recommendations | SI Supporting Information

ABSTRACT: Hydrogen peroxide (H$_2$O$_2$) is an effective green oxidant, which is used in many industrial processes. Here, the reaction mechanism for direct formation of H$_2$O$_2$ from H$_2$ and O$_2$ over Pd catalysts is studied using density functional theory calculations and mean-field kinetic modeling. The state of the catalyst as a function of reaction conditions is determined from *ab initio* thermodynamics. It is found that Pd is in a hydride phase during typical reaction conditions. Reaction landscapes are constructed for the reaction over PdH(111) and PdH(211). Formation of H$_2$O$_2$ instead of H$_2$O requires that O$_2$ adsorbs and that the surface intermediates O$_2$, OOH, and H$_2$O$_2$ do not dissociate. We find that these requirements are fulfilled on the stepped PdH(211) surface. Surface steps are needed for O$_2$ chemisorption as the adsorption on PdH(111) is endothermic. The high H coverage on the surface of the hydride is important to slow down the unwanted scission of the O−O bond and promote the desorption of the products. Comparative calculations for the Pd(111) surface show that this surface is inactive for both H$_2$O$_2$ and H$_2$O formation below room temperature for typical reaction mixtures. Our findings demonstrate the importance of surface steps and high hydrogen coverage for direct synthesis of H$_2$O$_2$ from H$_2$ and O$_2$ over Pd catalysts. The results imply that the selectivity of the reaction toward H$_2$O$_2$ is enhanced by a high partial pressure of H$_2$, which is in agreement with experimental observations.

KEYWORDS: H$_2$O$_2$, selectivity, Pd, PdH, DFT

INTRODUCTION

Hydrogen peroxide, H$_2$O$_2$, is a widely used oxidant for liquid-phase reactions within, for example, textile bleaching and waste water purification.[1] Hydrogen peroxide can oxidize organic compounds with H$_2$O and O$_2$ as the only byproducts.[2] This is a clear advantage with respect to nitric acid or chlorinated oxidizers, which may result in toxic byproducts.[2] Currently, the production of H$_2$O$_2$ is largely dependent on the anthraquinone oxidation process (AO process) with a series of reduction/oxidation steps.[3] This large-scale process requires the use of quinones and toxic organic solvents and energy-intensive purification procedures, generating undesirable wastes.[4] During the past decades, the direct synthesis of H$_2$O$_2$ from H$_2$ and O$_2$ over transition metals at low temperatures (275−315 K) has been explored as an appealing alternative production route thanks to its simplicity and low environmental impact. Moreover, these processes can be operated in a small/middle scale, and H$_2$O$_2$ can be produced close to the location of usage.[4,5]

Direct synthesis of H$_2$O$_2$ has not yet emerged at an industrial scale primarily because of its low selectivity toward H$_2$O$_2$.[6] The low selectivity comes mainly from irreversible O−O bond cleavage and the subsequent unselective hydrogenation of the intermediates to H$_2$O.[7] The reaction cycle following a Langmuir−Hinshelwood mechanism is shown in
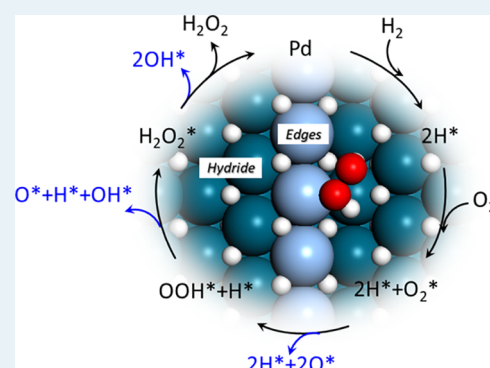
Figure 1. The cycle starts by adsorption of H$_2$ forming atomic hydrogen. The next step involves molecular adsorption of O$_2$. From this state, H$_2$O$_2$ can be formed by subsequent hydrogenation and eventual desorption of the product. The challenge is the unwanted O−O cleavage and subsequent H$_2$O formation. The O−O bond can be cleaved at different stages of hydrogenation, and the barrier for O−O rupture is reduced with an increasing degree of hydrogenation.

Palladium catalysts have shown higher selectivity for direct H$_2$O$_2$ synthesis than other transition-metal catalysts, such as Pt[8] and Au.[9] The highest selectivity reported to date for direct synthesis of H$_2$O$_2$ over catalysts of supported Pd nanoparticles is 80%.[1] However, the rate of H$_2$O$_2$ production selectivities appears to depend strongly on factors, such as reactant pressures,[10] particle size,[11] solvents (e.g., water and ethanol),[12] and promoters (e.g., the presence of halides).[4,13] In particular, the activity of the Pd catalysts has been found to depend strongly on the H$_2$/O$_2$ ratio and the reaction temperature.[12]

The literature concerning the H_2/O_2 ratio is, however, not conclusive. References[4,10,14] indicate that a high H_2/O_2 ratio is needed to enhance the H_2O_2 rate and selectivity, whereas refs[15,16] indicate that a H_2/O_2 ratio close to 1 gives the highest rate and selectivity. Regarding the effect of temperature, experimental studies agree that the H_2O_2 selectivity is favored at low temperatures.[12,17] It is known that O_2 dissociates above 200 K over metallic Pd.[18−20] This indicates that the active site for direct synthesis of H_2O_2 should be different from the metallic Pd state. However, the underlying mechanism for the reaction has not yet been well understood.

Improving the H_2O_2 selectivity over Pd catalysts would benefit from an atomic-level understanding of the reaction mechanism. Although H_2O_2 formation over Pd systems has been investigated from first principles,[7,21] we are not aware of studies where the hydride phase has been considered. Here, we investigate the reaction paths for direct formation of H_2O_2 from H_2 and O_2 over Pd catalysts by the combination of density functional theory calculations and first-principle-based kinetic modeling. Evaluation of reaction kinetics is needed to understand the kinetic consequences of different reaction paths. The state of the Pd catalysts under reaction conditions is determined by constructing a surface phase diagram with respect to the chemical potentials of H_2 and O_2. We find that Pd is preferably in a hydride state under typical reaction conditions. A high coverage of hydrogen is found to be important for the selectivity of the reaction as adsorbed hydrogen prevents O−O scission. The adsorption energy of O_2 is endothermic on PdH(111), which suggests that the reaction takes place over steps. We explore PdH(211) as a model for low-coordinated sites and find that O_2 adsorbs exothermically over this step and can be hydrogenated with low barriers. The kinetic analysis reveals a selectivity of about 0.3 over the PdH(211) step, which is in reasonable agreement with experiments.

■ COMPUTATIONAL METHODS

First-Principles Calculations. Spin-polarized density functional theory calculations are performed with the Vienna ab initio simulation package (VASP).[22−26] The Kohn−Sham orbitals are expanded with plane waves using a 450 eV energy cutoff, and the interaction between the valence electrons and the cores is described with the plane augmented wave approach.[27,28] The numbers of valence electrons considered in the calculations are 10 (Pd), 6 (O), and 1 (H). The exchange−correlation effects are described within the generalized gradient approximation according to Perdew, Burke, and Ernzerhof (PBE).[29] The D3 approach proposed by Grimme and co-workers[30,31] is added to describe the vdW interactions. The calculated lattice constants of bulk Pd and PdH within PBE + D3 are 3.89 and 4.08 Å, respectively, which agree well with the experimental values of 3.89 Å (Pd) and 4.09 Å (PdH).[32] Structures are optimized with the conjugate gradient method, and geometries are considered to be converged when the electronic energy difference between subsequent steps is lower than 1×10^{-5} eV and the largest force is lower than 0.03 eV/Å.

Pd and PdH surfaces are built from the theoretical lattice constants. The Pd(111) and PdH(111) surfaces are modeled by periodically repeated $p(3 \times 3)$ surface cells. The stepped PdH(211) surface is used to model the reactions over edge sites of typical Pd nanoparticles. The PdH(211) surface is considered using a $p(1 \times 2)$ surface cell. The PdH(211) step

joins (100) and (111) microfacets. All surface slabs are constructed with four-atomic layers, and repeated slabs are separated by 12 Å of vacuum. The Brillouin zone is sampled using the Monkhorst−Pack[33] scheme with a $4 \times 4 \times 1$ k-point for all considered surface cells. As the experimental stoichiometry of β-phase palladium hydride is $PdH_{0.7}$,[34] hydrogen atoms are randomly removed from the PdH surface slabs to obtain configurations with a H/Pd ratio of ∼0.7. H is preferably adsorbed at surface sites,[35] and the considered PdH surface slabs have a monolayer of H atoms on the surface.

Reaction barriers are calculated by the climbing image nudged elastic band technique as implemented in the transition-state tools of VASP.[36,37] Harmonic vibrational frequencies are computed using the finite-difference approach. The surface atoms are fixed during the vibrational analysis. The transition states are confirmed by vibrational analysis showing one imaginary frequency along the reaction coordinate. The vibrational analyses are also used to obtain zero-point-corrected energies.

The reaction energies $H_2 + 0.5\ O_2 \rightarrow H_2O$ and $H_2 + O_2 \rightarrow H_2O_2$ are calculated to be −2.28 and −1.19 eV, respectively. These results are in fair agreement with the experimental values[38] of −2.51 and −1.41 eV, respectively.

Surface Phase Diagram. A surface phase diagram with respect to the metal surface and surrounding gas reservoirs can be constructed to determine the stability of the considered systems. Here, the relative stabilities of H_2 and O_2 adsorption on Pd(111) structures are calculated by comparing the Gibbs free energy of adsorption (ΔG^{ads}). ΔG^{ads} is obtained with respect to the clean Pd(111) surface and evaluated as a function of the chemical potentials for H_2 (μ_{H_2}) and O_2 (μ_{O_2})

$$\Delta G^{ads} = \frac{1}{A}\left[G^{surf}_{N_HH,N_OO/Pd(111)} - G^{surf}_{Pd(111)} - \Delta N_{Pd}\mu^{bulk}_{Pd} \\ - \frac{N_O}{2}\mu_{O_2} - \frac{N_H}{2}\mu_{H_2} \right]$$

(1)

where A is the surface area, $G^{surf}_{N_HH,N_OO/Pd(111)}$ is the Gibbs free energy of Pd(111) with N_H-adsorbed H atoms and N_O-adsorbed O atoms, $G^{surf}_{Pd(111)}$ is the Gibbs free energy of clean Pd(111), and ΔN_{Pd} is the difference between the numbers of Pd atoms in the considered surface and the pristine surface. Surface reconstruction can lead to $\Delta N_{Pd} \neq 0$, and μ^{bulk}_{Pd} is calculated using the Pd bulk as a reservoir. The chemical potentials of H_2 (μ_{H_2}) and O_2 (μ_{O_2}) can be separated into a total energy term and terms dependent on temperature and pressure.[39] Thus, μ_{H_2} and μ_{O_2} are given by

$$\mu_x(T, P_x) = E_x + \Delta\mu_x(T, P^\circ) + k_BT \ln\left(\frac{P_x}{P^\circ}\right)$$

(2)

where x is either H_2 or O_2, P° is the standard pressure, and $\Delta\mu_x(T,P^\circ)$ is the chemical potential at the standard pressure. The stable structure at a given condition (T, P_{O_2}, and P_{H_2}) is given by the structure that minimizes ΔG^{ads}. The configurational entropy of the β-phase palladium hydride is estimated from[40]

$$\Delta S_{conf} = -Nk_B[x \ln(x) + (1 - x) \ln(1 - x)]$$

(3)

where x is 0.7 and N is the total number of octahedral sites. Thus, the free-energy contribution from the configurational entropy per site (G_{conf}) is given by

$$G_{conf} = -k_B T[x \ln(x) + (1 - x) \ln(1 - x)] \quad (4)$$

An extended palladium oxide bulk is thermodynamically stable when the oxygen content in the environment is high enough, which gives

$$\mu_{PdO}^{bulk} < \mu_{Pd}^{bulk} + \frac{1}{2}\mu_{O_2} \quad (5)$$

whereas a sufficient hydrogen content will make the reduction of PdO into H_2O and Pd preferred, which leads to

$$\mu_{Pd}^{bulk} + \mu_{H_2O} < \mu_{PdO}^{bulk} + \mu_{H_2} \quad (6)$$

Combining eqs 2, 5, and 6 gives the stability criterion for PdO in a mixed atmosphere of H_2 and O_2

$$\Delta\mu_{H_2} - \frac{1}{2}\Delta\mu_{O_2} < -2\Delta E_{PdO}^f + \Delta E_{H_2O}^f \quad (7)$$

Here, ΔE_{PdO}^f is the formation energy of PdO at 0 K and $\Delta E_{H_2O}^f$ is the formation energy of H_2O from H_2 and O_2.

Microkinetic Modeling. The reaction kinetics is obtained by mean-field microkinetic modeling. The reaction networks are constructed from our proposed reaction mechanism (see below). A set of coupled ordinary differential equations (ODEs) describes the time-dependent coverage of each species[41]

$$\frac{d\theta_i}{dt} = \sum_j r_j(\vec{\theta}) n_{j,i} \quad (8)$$

where θ_i is the fractional coverage of species i, $r_j(\vec{\theta})$ is the rate of reaction j, which depends on the coverages of all species, and $n_{j,i}$ is the stoichiometric coefficient of species i in reaction j. Microkinetic models often have rate constants that differ by many orders of magnitude, which makes the system of ODEs stiff. In this work, a method based on backward differentiation formulas within the VODE solver in SciPy[42] has been used to numerically integrate the system of ODEs until the steady state is reached.

The rate constants k for the surface reactions are calculated through transition-state theory[43]

$$k = \frac{k_B T}{h} \exp\left(\frac{\Delta S^{\#}}{k_B}\right) \exp\left(\frac{-\Delta E^{\#}}{k_B T}\right) = A_f \exp\left(\frac{-\Delta E^{\#}}{k_B T}\right) \quad (9)$$

where $\Delta S^{\#}$ and $\Delta E^{\#}$ are the entropy and electronic energy differences between the transition state and the reactant, respectively. The entropies for the adsorbed species are calculated within the harmonic approximation, where the translations and rotations are treated as frustrated vibrations.[44] A_f defines the pre-exponential factor for the forward reaction. The rate constants for the (non-activated) adsorption reactions are calculated according to collision theory

$$k_{ads} = \frac{P_x s_0 a_{site}}{\sqrt{2\pi m k_B T}} = P_x A_f \quad (10)$$

where P_x is the partial pressure of x, s_0 is the sticking coefficient at zero coverage, a_{site} is the area of an adsorbed site, and m is the mass of the molecule. s_0 is assumed to be unity for all cases. Thermodynamic consistency is enforced in the model by calculating the reverse rate constants from the equilibrium constants for all steps.

For the interactions between the adsorbed species, it is found that the majority of the interactions is repulsive with the exception of the OH−OH interaction. We have included O−O and OH−OH interactions following ref 45. The H−H interactions are modeled in a linear fashion, as seen in the Supporting Information. The interactions between adsorbed O_2 molecules are found to be small and, therefore, neglected in the model.

RESULTS

The direct synthesis of H_2O_2 from H_2 and O_2 proceeds over Pd catalysts at low temperatures (275−315 K) and reactant pressures normally in the range of 0.5−10 MPa H_2 and 0.5−10 MPa O_2.[4,14] At these pressures and temperatures, exposure of Pd to only H_2 would result in the formation of palladium hydride (α- or β-phase).[34,46,47] Similarly, the exposure of Pd to O_2 at these temperatures results initially to adsorbed oxygen and thereafter a two-dimensional surface oxide.[48,49] Formation of bulk oxide requires for kinetic reasons higher temperatures.[48] During H_2O_2 formation, Pd is exposed to both H_2 and O_2, which implies that it is important to investigate the stable surface structure with the relevant gas mixture.

State of the Catalyst. The stability of the calculated surface structures in equilibrium with gas-phase H_2 and O_2 is compared by evaluating the Gibbs free energy. Here, we have considered clean Pd(111), a $p(3 \times 3)$ overlayer of atomic oxygen on Pd(111), Pd_5O_4 surface oxide[48] on Pd(111), the PdO bulk, a $p(3 \times 3)$ overlayer of atomic hydrogen on Pd(111), and a $p(3 \times 3)$ β-phase palladium hydride (111) [$PdH_{0.7}(111)$]. The considered structures focus on the state of the catalyst, being a metal, an oxide, or a hydride. The actual surface coverages, which are determined by both thermodynamics and reaction kinetics, are obtained by mean-field kinetic modeling as described below.

The stable phases at the corresponding H_2 and O_2 chemical potentials are shown in Figure 2. The clean Pd(111) surface is the stable phase when the H_2 and O_2 chemical potentials are low. If the H_2 chemical potential is kept low and O_2 chemical potential increases (along the y-axis) to oxygen-rich conditions, first a $p(3 \times 3)$ overlayer appears on the Pd(111) surface, then a Pd_5O_4 surface oxide, and finally the PdO bulk oxide. The structure of the surface oxide has been determined by *in situ* surface X-ray diffraction and core-level spectroscopy measurements.[48] If the O_2 chemical potential is kept low and the H_2 chemical potential gradually increases (along the x-axis), a completely H-covered Pd(111) surface is first formed and, thereafter, the β-phase palladium hydride ($PdH_{0.7}$). This is in good agreement with experimental results[34,47] (at low temperatures, Pd goes directly between the metallic phase and β-phase[50]). The adsorption energy for hydrogen in the bulk is significantly lower than the adsorption energy on the surface,[35] which implies that hydrogen will first occupy adsorption sites on the surface and only occupy bulk sites once a full surface coverage is obtained.

The relevant operating conditions during H_2O_2 synthesis over Pd are indicated by the white square in Figure 2 (P_{H_2}, P_{O_2} = 0.5−10 MPa, and T = 275−315 K). The region of the square is situated in the β-hydride phase close to the boundary to the Pd_5O_4 surface oxide. Our results show that the β-hydride phase should be considered as the most abundant surface structure during H_2O_2 formation conditions, particularly when H_2 is fed in excess. This finding is in accord with experimental X-ray

absorption spectroscopy data,[16] showing that the β-phase PdH is present for H_2/O_2 ratios > 1.
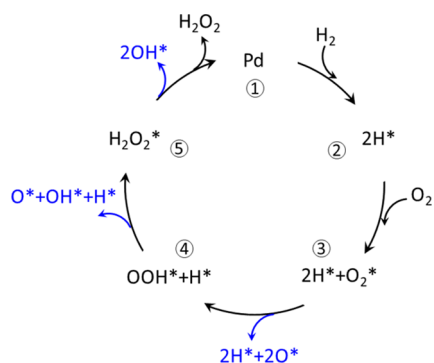

Figure 1. Schematic reaction cycle for direct formation of H_2O_2 from H_2 and O_2.

Reaction Paths over Pd(111) and PdH(111). The reaction paths for direct H_2O_2 formation from H_2 and O_2 on Pd(111) and β-PdH(111) are shown in Figures 3 and 4, respectively. Even though the β-hydride is the preferred phase during the reaction conditions, we consider the clean Pd(111) surface as a comparison. On Pd(111), O_2 is first adsorbed in a molecular state over an fcc hollow site (O*O*). H_2 is subsequently adsorbed and dissociated (O*O* + 2H*). The dissociated atomic H atoms can react with O*O*, forming an O*O*H species with a barrier of 0.54 eV. Thereafter, adsorbed hydrogen peroxide (HO*OH) can be formed with a high barrier of 0.86 eV. The surface hydrogen peroxide desorbs in the last step from the surface. The desorption energy is 0.60 eV. However, there are a couple of possible side reactions along the potential energy landscape. O_2 can dissociate with an activation energy of 0.63 eV, forming two oxygen atoms on the surface (2O*). Adsorbed O and H can react to form O*H with a barrier of 0.98 eV (not shown in the figure). Another side reaction is the dissociation of the O*O*H species to an O* and an O*H. This reaction has a small barrier of 0.11 eV. A water molecule can be formed by reaction between O*H and H* with a barrier of 0.49 eV. The desorption energy of water is 0.45 eV. A third side reaction is the dissociation of surface HO*OH to two O*H groups, which is exothermic and has a small barrier of 0.11 eV.

All our calculated energies for this reaction on Pd(111) are in good agreement with the previous studies.[7,21] Note that water should mainly be formed by the reaction between two OH groups or hydrogenation of HO*OH. The hydrogenation of HO*OH over Pd(111) is not considered as it is difficult to form HO*OH over Pd(111). The barrier for direct O_2 dissociation over Pd(111) is high enough to hinder direct dissociation into 2O* below room temperature. Moreover, the barrier for OH formation from atomic oxygen and hydrogen is high. This is consistent with the observation that OH groups are formed from O* and H* at step sites.[51]

Turning to the reaction paths on β-PdH(111) (Figure 4), the reaction landscape is more complicated than on clean Pd(111) due to the high coverage of the surface hydrogen and the existence of the bulk hydrogen. H_2 is first dissociated on the surface, and the surface is thereafter fully covered by the hydrogen atoms. O_2 is found to be physisorbed in a triplet state with an adsorption energy of 0.16 eV. The barrier to form a chemisorbed molecule in the singlet state is 0.61 eV. The direct dissociation of O_2 has a large barrier of 1.12 eV. With chemisorbed O_2, there are two paths to form OOH species. One is to form HO*O with one bond to the surface, which has a barrier of 0.22 eV. The other species (O*O*H) has two bonds to the surface and is formed with a lower barrier of 0.12
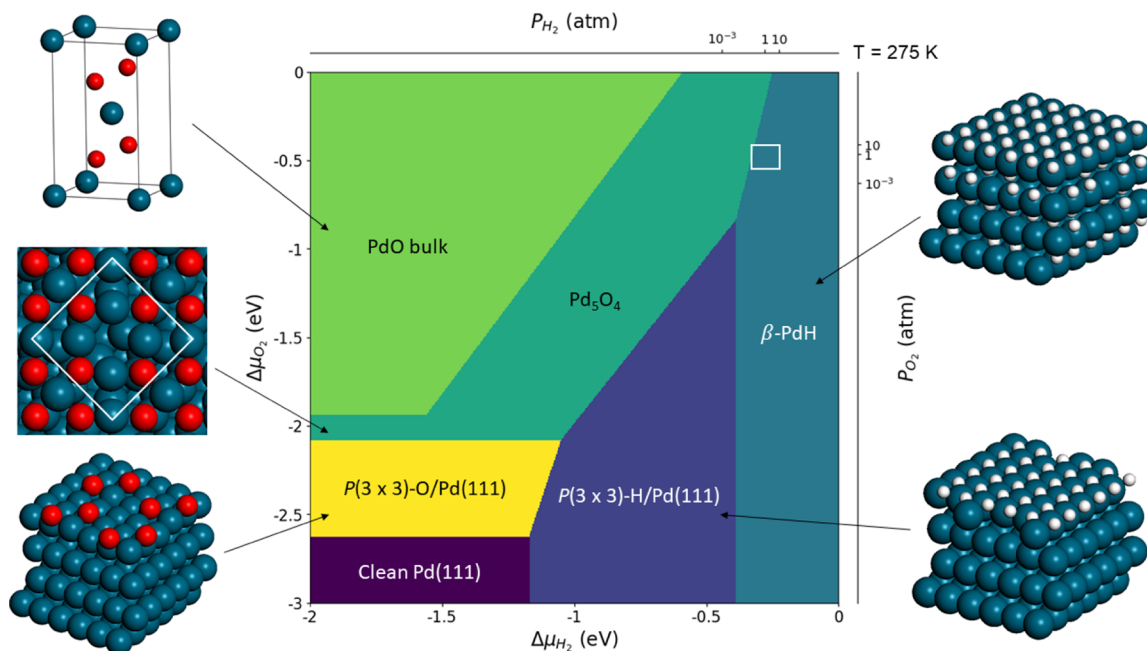

Figure 2. Surface phase diagram of Pd(111) in constrained thermodynamic equilibrium with gas-phase H_2 and O_2. The phase diagram is given with respect to the chemical potentials of H_2 and O_2. The corresponding H_2 (O_2) pressure at 275 K is shown in the black bar at the top (right) of the axis. The white square in the phase diagram denotes the typical gas conditions of direct H_2O_2 formation [P_{H_2}, P_{O_2} = 0.5−10 MPa, T = 275−315 K; atom color codes: Pd (blue), O (red), and H (white)].
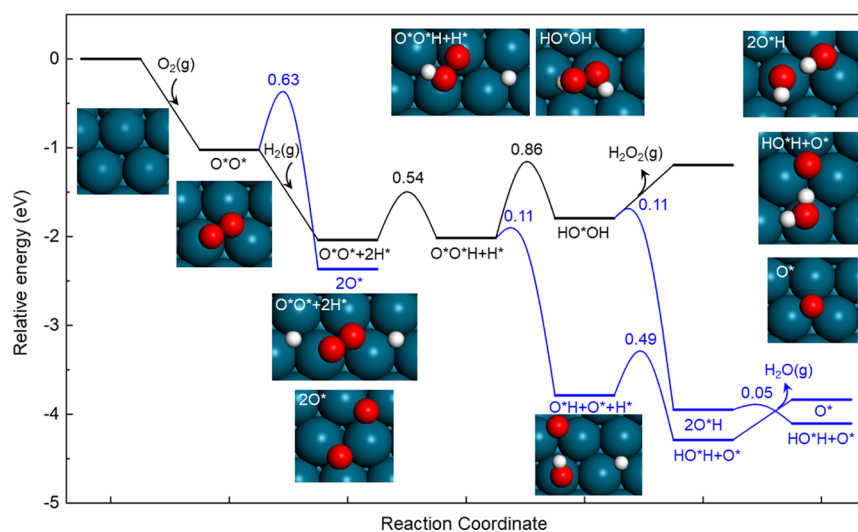
Figure 3. Potential energy landscape for direct H_2O_2 formation from H_2 and O_2 over Pd(111). The lines with the blue color represent the path toward the side reactions. All energies are zero-point-corrected. Atom color codes: Pd (blue), O (red), and H (white).
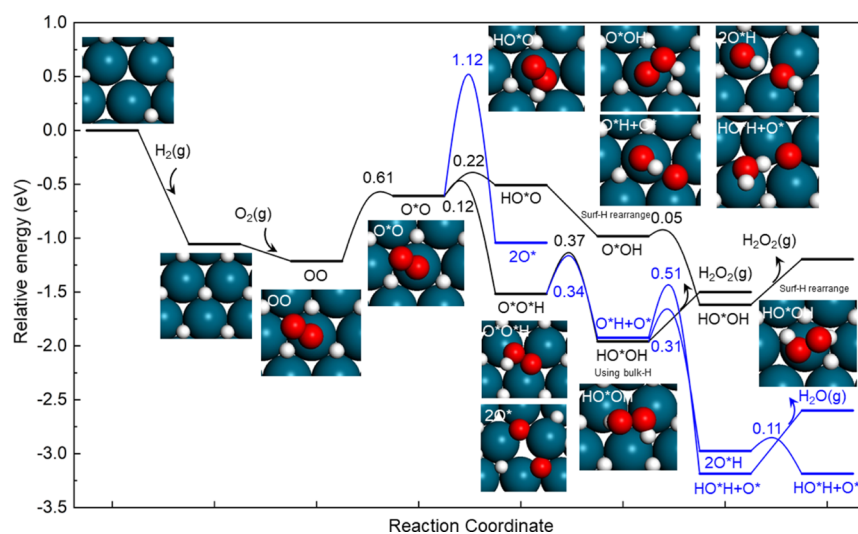

Figure 4. Potential energy landscape for direct H_2O_2 formation from H_2 and O_2 on β-PdH(111). The lines with the blue color represent the path toward the side reactions. Steps marked with surface-H rearrangement indicate that the surrounding hollow sites of the surface species are all covered by surface H. All energies are zero-point-corrected. Atom color codes: Pd (blue), O (red), and H (white).

eV. To continue the reaction with HO*O, the species need to reorient and bind with the unhydrogenated oxygen atom to the surface (O*OH). This step is spontaneous with a full hydrogen coverage, which is maintained by either diffusion of H from the bulk or hydrogen adsorption. In the potential energy diagram, a local full coverage is kept by moving a surface hydrogen atom close to HO*O. HO*OH is formed from O*OH with a small barrier of 0.05 eV. The desorption energy of the adsorbed HO*OH is 0.38 eV. HO*OH can also be formed from O*O*H by reaction with a subsurface hydrogen (e.g., bulk-dissolved H) with a small barrier of 0.37 eV. This is preferred with respect to a reaction with an adjacent surface hydrogen. The desorption energy of this HO*OH species is 0.38 eV.

The side reactions involve dissociation of the O*O*H species into an O*H group and an adsorbed O*, having a barrier of 0.34 eV. Another side reaction is the dissociation of HO*OH, which proceeds with a barrier of 0.31 eV. This path is possible if there are free sites on the surface to accommodate

2O*H. Water can be formed either with a barrier of 0.51 eV from O*H and H* or, alternatively, with a smaller barrier of 0.11 from 2O*H. Note that the dissociation of O*O*H and HO*OH requires higher barriers on the hydride PdH(111) than on the clean Pd(111) surface. This indicates that the presence of surface H should increase the selectivity toward H_2O_2. However, the potential energy landscape in Figure 4 also shows that the O_2 adsorption step is endothermic, making H_2O_2 formation a very slow process.

We find that the interaction of O_2 with Pd(111) and β-PdH(111) is significantly different. O_2 binds to Pd(111) by -1.02 eV, whereas the reaction is endothermic on β-PdH(111). There are two main reasons for the difference. One is the change in Pd electronic structure upon hydride formed. The densities of states of Pd, $PdH_{0.7}$, and PdH bulk are reported in the Supporting Information. The width of the d-band is reduced and shifted to lower energies as the hydride is formed. Moreover, d-states are depleted from the Fermi level. These are changes that reduce the interaction with O_2.[52] In
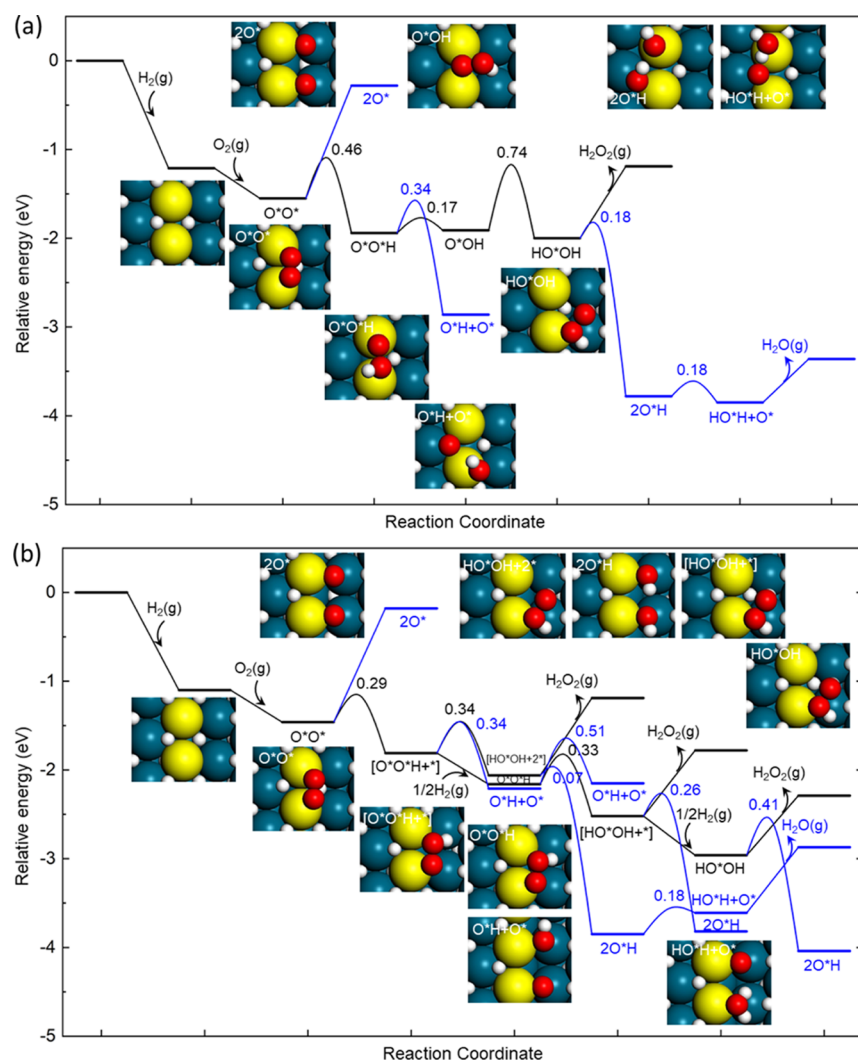
Figure 5. Potential energy landscape for direct H_2O_2 formation from H_2 and O_2 on β-PdH(211). Two types of adsorbed H may take part in the reactions: (a) H on the (111) microfacet and (b) H on the (100) microfacet. The lines with the blue color represent the path toward the side reactions. All energies are zero-point-corrected. Pd atoms at the step edge are highlighted with the yellow color. Atom color codes: Pd (blue), O (red), and H (white).

addition, the H is slightly negatively charged in the hydride, which results in a repulsion to O_2 upon adsorption.

Reaction Paths over PdH(211). Direct synthesis of H_2O_2 is typically performed over Pd nanoparticles, which have undercoordinated edge and corner sites. It is known that low-coordinated sites may strongly influence the activity.[53] To simulate the reactions on the edge sites of a PdH nanoparticle, here, H_2O_2 formation has been investigated on the stepped PdH(211) surface, as seen in Figure 5. Owing to the low-coordinated Pd atoms on the edges, O_2 adsorbs on this surface by −0.35 eV. The dissociation of O*O* on the stepped surface with a full coverage of hydrogen is strongly endothermic by 1.27 eV, which implies that direct dissociation is hindered under reaction conditions. After the adsorption of O_2, there are two possible routes for OOH formation. One route uses the H* from the (111) microfacet (Figure 5a), and the other uses the H from the (100) microfacet (Figure 5b).

Following the path in Figure 5a, O*O*H formation proceeds via a barrier of 0.46 eV. The subsequent formation of HO*OH involves two steps. First, O*O*H reorients with a barrier of 0.17 eV to allow for a reaction with the second H* on the (111) microfacet. Second, HO*OH is formed with a

barrier of 0.74 eV. A side reaction is at this point dissociation of O*O*H into O*H and O*. The barrier for this reaction is 0.34 eV. Moreover, adsorbed HO*OH is found to dissociate easily with a barrier of 0.18 eV. HO*H can be formed from two O*H groups, a process that has a barrier of 0.18 eV. The desorption of HO*OH and HO*H from the edges is less facile than the desorption on the Pd(111) surface due to their stronger binding energies.

Turning to the path in Figure 5b, the O*O*H formation from O*O* and the H* on the (100) microfacet requires a smaller barrier (0.29 eV) than the formation using H on the (111) microfacet (0.46 eV). The more facile transport of H from the (100) microfacet can be explained by a 0.1 eV weaker bond to the surface. After the formation of O*O*H, there are three possibilities for the following reactions: (i) HO*OH can be formed via a barrier of 0.34 eV. HO*OH can either desorb by 0.86 eV or dissociate into two O*H groups via a small (0.07 eV) barrier. The two O*H groups can react with each other, forming a HO*H species by a barrier of 0.18 eV. The desorption of HO*H is endothermic by 0.74 eV. (ii) O*O*H can dissociate to O*H + O* with a barrier of 0.34 eV. (iii) As empty sites are formed upon O*O*H formation, it is feasible

Table 1. Considered Elementary Reaction Steps on PdH(211) with H Transferred from the (100) Microfacet[a]

no.	reaction equation	E_f (eV)	A_f	E_b (eV)	A_b
(1)	$H_2(g) + 2* \leftrightarrow 2H*$	0.00	1.06×10^3	1.03	8.84×10^7
(2)	$O_2(g) + 2*(edge) \leftrightarrow O*O*(edge)$	0.00	2.67×10^3	0.36	1.30×10^{10}
(3)	$O*O*(edge) + H* \leftrightarrow [O*O*H(edge) + *]$	0.29	2.77×10^{12}	0.65	1.90×10^{12}
(4)	$O*O*(edge) + 2* \leftrightarrow 2O* + 2*(edge)$	1.28	2.57×10^{12}	0.00	1.28×10^{13}
(5)	$[O*O*H(edge) + *]_{str1} + H* \leftrightarrow [HO*OH(edge) + 2*]_{str1} + *(edge)$	0.34	2.83×10^{12}	0.60	1.15×10^{12}
(6)	$[O*O*H(edge) + *]_{str1} + * \leftrightarrow O*H + O* + 2*(edge)$	0.34	1.67×10^{12}	0.74	5.18×10^{12}
(7)	$[O*O*H(edge) + *]_{str1} + H_2(g) + * \leftrightarrow [O*O*H(edge)]_{str2} + 2H*$	0.00	1.06×10^3	0.70	2.91×10^5
(8)	$[HO*OH(edge) + 2*]_{str1} \leftrightarrow H_2O_2(g) + 2* + *(edge)$	0.87	6.80×10^{15}	0.00	2.59×10^2
(8′)	$[HO*OH(edge) + 2*]_{str1} \leftrightarrow H_2O_2(l) + 2* + *(edge)$	0.42	5.65×10^6	0.00	2.59×10^2
(9)	$[HO*OH(edge) + 2*]_{str1} \leftrightarrow O*H + O*H + *(edge)$	0.07	2.16×10^{12}	1.86	1.11×10^{13}
(10)	$[O*O*H(edge)]_{str2} + H* \leftrightarrow [HO*OH(edge) + *]_{str2} + *(edge)$	0.33	2.95×10^{12}	0.69	1.33×10^{12}
(11)	$[HO*OH(edge) + *]_{str2} \leftrightarrow H_2O_2(g) + * + *(edge)$	0.74	6.80×10^{15}	0.00	2.59×10^2
(11′)	$[HO*OH(edge) + *]_{str2} \leftrightarrow H_2O_2(l) + * + *(edge)$	0.29	5.65×10^6	0.00	2.59×10^2
(12)	$[O*O*H(edge)]_{str2} + 2* \leftrightarrow O*H + O* + 2*(edge)$	0.51	3.78×10^{12}	0.50	1.69×10^{13}
(13)	$[HO*OH(edge) + *]_{str2} + H_2(g) + * \leftrightarrow [HO*OH(edge)]_{str3} + 2H*$	0.00	1.06×10^3	0.88	3.17×10^5
(14)	$[HO*OH(edge)]_{str3} \leftrightarrow H_2O_2(g) + *(edge)$	0.67	7.34×10^{15}	0.00	2.59×10^2
(14′)	$[HO*OH(edge)]_{str3} \leftrightarrow H_2O_2(l) + *(edge)$	0.22	6.11×10^6	0.00	2.59×10^2
(15)	$[HO*OH(edge)]_{str3} + 2* \leftrightarrow O*H + O*H + *(edge)$	0.41	2.41×10^{12}	1.49	1.63×10^{13}
(16)	$O*H + O*H + *(edge) \leftrightarrow HO*H(edge) + O* + *$	0.18	4.10×10^{12}	0.04	1.79×10^{12}
(17)	$HO*H(edge) \leftrightarrow H_2O(g) + *(edge)$	0.74	1.36×10^{15}	0.00	3.56×10^2
(17′)	$HO*H(edge) \leftrightarrow H_2O(l) + *(edge)$	0.29	2.20×10^6	0.00	3.56×10^2
(18)	$O* + H* \leftrightarrow O*H + *$	0.69	4.25×10^{12}	1.19	2.58×10^{12}
(19)	$O*H + H* + *(edge) \leftrightarrow HO*H(edge) + 2*$	0.58	5.38×10^{12}	0.96	1.25×10^{12}
(20)	$[HO*OH(edge) + *]_{str2} + * \leftrightarrow O*H + O*H + *(edge)$	0.26	2.08×10^{12}	1.56	9.52×10^{12}

[a]The forward (E_f) and backward (E_b) energy barriers are reported with zero-point corrections. The desorption steps with a prime denote the desorption into the liquid state. As the reaction network has different structures of O*O*H and HO*OH, we denote the different possibilities by $[O*O*H(edge) + *]_{str1}$, $[O*O*H(edge)]_{str2}$, $[HO*OH(edge) + 2*]_{str1}$, $[HO*OH(edge) + *]_{str2}$, and $[HO*OH(edge)]_{str3}$. The different structures are shown in the Supporting Information.

to fill this site either by H diffusion or by H_2 adsorption, yielding a full coverage. In Figure 5b, the empty site is filled by H_2 adsorption. The high coverage of H on the (100) microfacet makes the dissociation of O*O*H less facile than the formation of HO*OH. The dissociation has a barrier of 0.51 eV, whereas HO*OH is formed by a barrier of 0.33 eV. The formation of HO*OH gives rise to an empty site, and the dissociation of HO*OH to two O*H groups is associated with a barrier of 0.26 eV. Once HO*OH is formed, the full coverage can be maintained by yet another H_2 adsorption step. The dissociation of HO*OH to two O*H groups on the edges with a high H coverage has a barrier of 0.41 eV. The barrier for the dissociation of HO*OH to two O*H groups increases from 0.07 to 0.41 eV with increasing surface H coverage. This shows that a high H coverage slows down the dissociation. Moreover, the desorption of HO*OH is endothermic by 0.67 eV. The full coverage of H reduces the desorption energy of HO*OH on the edges. The desorption energies with one or two hydrogen vacancies close to HO*OH are calculated to be 0.74 and 0.86 eV, respectively.

Microkinetic Analysis. The relevance of the proposed reaction landscape can be verified by performing a microkinetic analysis with the calculated kinetic parameters. In the microkinetic simulations, the partial pressures of H_2 and O_2 are chosen to be 1 atm. The H_2O_2 and H_2O pressures are set to close to 0. The temperatures for the simulations are ramped from 275 to 315 K, which is within the experimental regime.[4]

The microkinetic simulations for the direct H_2O_2 formation provide information on both the rate of product formation and the coverages of the surface species and have been performed for the potential energy surfaces for PdH(111) (Figure 4) and

PdH(211) (Figure 5), respectively. We find that no H_2O_2 is formed over PdH(111) in the studied temperature interval. The kinetic bottleneck is the adsorption of O_2. The results for PdH(111) are reported in the Supporting Information. For the PdH(211) surface, the use of H atoms from the (111) microfacet involves a high barrier, which prevent facile H_2O_2 formation (see the Supporting Information). Here, we concentrate on the results for the PdH(211) surface where H atoms are transferred from the (100) microfacet. The reaction barriers and pre-exponential factors (at 275 K) for forward and backward reactions between the adsorbed O_2 and H on the (100) microfacet are listed in Table 1. The parameters for H_2O_2 and H_2O desorption have been adjusted to account for the fact that the desorption is to the liquid phase. In particular, experimental heats of vaporization and liquid-state entropies are used (see the Supporting Information).[38]

The pre-exponential factors (at 275 K) for forward and backward reactions are denoted by A_f and A_b, respectively. The pre-exponential factors for surface reactions and desorption events are given in (1/s). The pre-exponential factors for adsorption are given in ($Pa^{-1} s^{-1}$). Species with (edge) denote the adsorption sites on the edges.

The turnover frequency (TOF) is given by the rate of the formation of the product. Figure 6 shows the TOF of the formation of H_2O_2 and H_2O as a function of temperature. We find that the TOF for the formation of H_2O_2 is lower than the TOF for H_2O formation in the entire temperature interval. H_2O_2 formation has a maximum at 295 K, whereas the H_2O rate monotonically increases with temperature. The reason for the decrease in TOF for H_2O_2 is the onset of the H_2O_2
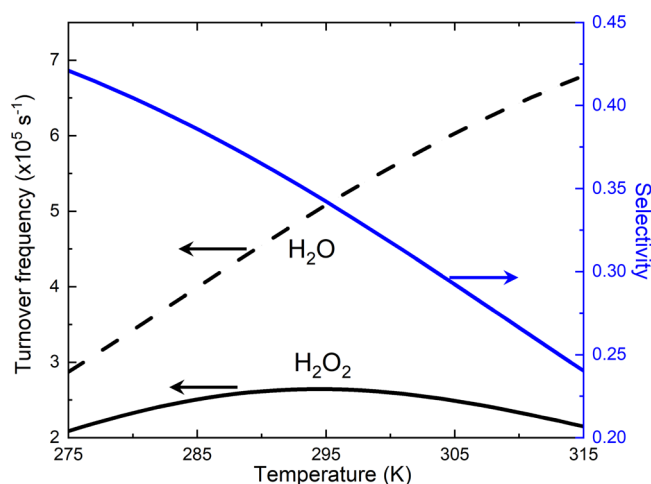
Figure 6. TOF for H_2O_2 and H_2O formation on the stepped surface PdH(211) as a function of temperature. The selectivity toward the formation of H_2O_2 is given in blue. The pressures of H_2 and O_2 are both 1 atm.

decomposition into OH groups. The TOF of H_2O_2 formation shows a moderate dependence on temperature in the range of 278–288 K, which agrees with experiments.[14] Moreover, the decrease in H_2O_2 formation at higher temperatures (above ~305 K) due to HO*OH decomposition is also in agreement with experiments.[17,54]

The selectivity toward H_2O_2 formation ($S_{H_2O_2}$) is defined as

$$S_{H_2O_2} = \frac{TOF_{H_2O_2}}{TOF_{H_2O_2} + TOF_{H_2O}} \quad (11)$$

where $TOF_{H_2O_2}$ and TOF_{H_2O} are the TOFs for H_2O_2 and H_2O formation, respectively. The corresponding selectivity at each temperature is given in Figure 6. The selectivity toward H_2O_2 formation decreases with increasing temperature. This implies that direct H_2O_2 formation should be performed at low temperatures to reach high selectivity. This finding is consistent with the experimental data.[5,14,54] The reaction order in H_2 is calculated to increase from 0.3 to 0.7 as the temperature is increased. The reaction order in O_2 is calculated to be negative (about −0.2) in the studied temperature interval. The reaction order in H_2 has been measured to be either 0.5[10] or 1.0.[14] The reaction order in O_2 was in ref 10 measured to be slightly negative. We have also performed a degree of rate control (DRC)[55] analysis (Figure S7 in the Supporting Information). H_2 adsorption and HO*OH formation from O*O*H have a positive DRC as well as H_2O desorption. Instead, HO*OH dissociation into 2O*H has a negative DRC.

■ DISCUSSION

In the results, we identify three key findings important for the mechanism of direct H_2O_2 synthesis: (i) the Pd catalyst exists in its hydride form under typical direct synthesis conditions; (ii) H_2O_2 selectivity is significantly improved on the hydride thanks to a combination of facile H addition and suppression of water formation; and (iii) H_2O_2 synthesis rates are much higher on edge sites than on Pd particle terraces. Below, we elaborate on these conclusions and discuss them in the context of prior experimental work.

Recent X-ray absorption experiments show that under H_2/O_2 ratios larger than 1, hydride is present under reaction conditions and that a phase transition to an oxide-terminated metal surface takes place as the H_2/O_2 ratio is lowered.[15] This agrees with the presented phase diagram. Experimentally, the oxide surface also shows some selectivity toward H_2O_2 synthesis.[16] The mechanism for the activity of the oxide surface could be related to the mechanism for the hydride surface, for example, a completely oxidized surface disfavors O−O bond rupture.

Hydrides have previously been found to be associated with higher selectivity for direct H_2O_2 synthesis.[4,6] The results reported here provide insights into the reasons for these observations. One possible explanation for the importance of the hydride is associated with a high H coverage on the surface, which prevents the side reactions and facilitates the desorption of HO*OH, as shown in the reaction landscapes. Compared with the potential energy landscape on clean Pd(111), the coverage of the surface hydrogen plays an important role to prevent the side reactions on β-PdH(111). With the full coverage of hydrogen on β-PdH(111), O_2 prefers to be adsorbed as O*O species and the dissociation is kinetically hindered by a higher activation energy of 1.12 eV. This kind of site blocking created by surface H atoms would also hypothetically be observed for other types of surface adsorbates. Long-chain ligands, such as alkanethiols[56−58] and alkyl ammonium phosphates,[7] have been found to improve H_2O_2 yields, likely by suppressing the undesired O−O bond breaking. In addition to inhibiting O−O dissociation reactions, the presence of a hydride phase promotes H addition reactions. Keeping the molecular oxygen (O*O) on the surface promotes the formation of surface OOH species. The barriers for OOH formation are lower than those on clean Pd(111). In addition, having a high coverage of surface hydrogen also makes the formation of HO*OH from HO*O more facile than on clean Pd(111); the barrier is calculated to be only 0.05 eV on the hydride. The spontaneous desorption of HO*OH from a surface with high H coverage implies that surface hydrogen also prevents the dissociation of HO*OH. Moreover, the formation of HO*OH from O*O*H species by using subsurface hydrogen shows that bulk-dissolved hydrogen in Pd can promote the direct formation of H_2O_2.

The importance of the reactant pressure for the selectivity of H_2O_2 production was first found experimentally by Lunsford.[59] Recently, Wilson and Flaherty[10] observed that the rate of H_2O_2 production increases dramatically with the H_2 pressure keeping the O_2 pressure fixed. On the contrary, increasing the O_2 pressure with a fixed H_2 pressure did not result in a changed rate for H_2O_2 formation. This is an indication that the state of the catalyst, being in either a hydride state or an oxide state, is critical for the selectivity to H_2O_2.

Even though the barriers for OOH and HOOH formation are low on the PdH(111) surface, the endothermic adsorption of O_2 on PdH(111) leads to a very low predicted reaction rate. Thus, hydrogen-covered (111) terraces of large Pd nanoparticles should, in principle, be inert for direct H_2O_2 production. Instead, the undercoordinated atoms at the edge of a stepped surface provide sites for O_2 adsorption and facile H_2O_2 formation. Our finding highlights the importance of undercoordinated sites in typical Pd nanoparticles for the direct synthesis of H_2O_2. This hypothesis appears to accord with recent observations of enhanced H_2O_2 direct synthesis for catalysts with Pd clusters below 2 nm[11] as well as earlier

reports of an enhanced yield for palladium nanoparticles with a high number undercoordinated sites.[5]

We note that it has been suggested that H_2O_2 can be formed via sequential protonation of adsorbed O_2 and OOH from H^+ in the solution.[10] In ref 10, it was found that the H_2O_2 formation rates require H^+ in the solution and that the rate increased with addition of H^+ donors (e.g., H_2SO_4, HCl, or H_2CO_3), whereas rates for H_2O_2 formation are low in aprotic solvents. We have performed calculations of the diffusion barrier of the adsorbed H^* to an adsorbed water layer forming H_3O^+ over PdH(111). The calculations show that the barrier is small (about 0.4 eV, see the Supporting Information), and we believe that such proton−electron transfer mechanisms could work in parallel with the reaction paths we have discussed here.

CONCLUSIONS

Herein, we provide a perspective on the reaction mechanism for direct formation of H_2O_2 from H_2 and O_2 over Pd catalysts by the combination of density functional theory calculations and mean-field kinetic modeling. First, the state of the Pd catalyst under different reaction conditions has been determined by constructing a surface phase diagram with respect to the chemical potential of H_2 and O_2 at 275 K. It is found that β-PdH(111) with full coverage of hydrogen is the stable phase with 1 atm H_2 and 1 atm O_2. Thus, the reaction steps for H_2O_2 formation on Pd(111) and β-PdH(111) are investigated. To model the reactions on the edge sites in a typical Pd nanoparticle, a stepped surface PdH(211) is employed to construct the reaction landscape. It is found that adsorption of O_2 is endothermic on PdH(111), which results in low H_2O_2 production over the extended facet. However, the edge sites of the stepped surface PdH(211) provide sites to adsorb O_2 exothermically, which gives possibilities for H_2O_2 formation. Additionally, the decomposition of the intermediate species to OH groups is kinetically hindered by site blocking of neighboring surface H. The surface hydrogen is, moreover, found to facilitate the desorption of H_2O_2, which further prevents the unwanted decomposition of H_2O_2. Our findings suggest that undercoordinated sites are active sites for direct H_2O_2 formation and highlight the importance of hydrogen coverage on the Pd catalyst surface. The results imply that the selectivity of the reaction toward H_2O_2 can be enhanced by a high partial pressure of H_2. In this way, we provide a mechanistic understanding of the intrinsic role of the reactant pressure and the role of undercoordinated sites for direct synthesis of H_2O_2 on Pd catalysts.

ASSOCIATED CONTENT

Supporting Information

The Supporting Information is available free of charge at https://pubs.acs.org/doi/10.1021/acscatal.0c05548.

> Comparison between electronic densities of states for Pd and PdH, scaling relation for H−H interaction in the kinetic model, reaction networks, equilibrium coverages, reaction orders, analysis of DRC, and mechanism for H transfer via an adsorbed water layer (PDF)

AUTHOR INFORMATION

Corresponding Authors

Lin Chen − *Department of Physics and Competence Centre for Catalysis, Chalmers University of Technology, SE-412 96 Göteborg, Sweden;* orcid.org/0000-0002-7905-9587; Email: clin@chalmers.se

Henrik Grönbeck − *Department of Physics and Competence Centre for Catalysis, Chalmers University of Technology, SE-412 96 Göteborg, Sweden;* orcid.org/0000-0002-8709-2889; Email: ghj@chalmers.se

Author

J. Will Medlin − *Department of Chemical and Biological Engineering, University of Colorado Boulder, Boulder 80303, Colorado, United States;* orcid.org/0000-0003-2404-2443

Complete contact information is available at:
https://pubs.acs.org/10.1021/acscatal.0c05548

Notes
The authors declare no competing financial interest.

REFERENCES

(1) Edwards, J. K.; Solsona, B.; N, E. N.; Carley, A. F.; Herzing, A. A.; Kiely, C. J.; Hutchings, G. J. Switching off hydrogen peroxide hydrogenation in the direct synthesis process. *Science* **2009**, *323*, 1037−1041.

(2) Noyori, R.; Aoki, M.; Sato, K. Green oxidation with aqueous hydrogen peroxide. *Chem. Commun.* **2003**, *16*, 1977−1986.

(3) Goor, G.; Glenneberg, J.; Jacobi, S. Hydrogen Peroxide. *Ullmann's Encyclopedia of Industrial Chemistry*; American Cancer Society, 2012; Vol. *18*, pp 393−427.

(4) Flaherty, D. W. Direct synthesis of H_2O_2 from H_2 and O_2 on Pd catalysts: Current understanding, outstanding questions, and research needs. *ACS Catal.* **2018**, *8*, 1520−1527.

(5) Campos-Martin, J. M.; Blanco-Brieva, G.; Fierro, J. L. G. Hydrogen peroxide synthesis: an outlook beyond the anthraquinone process. *Angew. Chem., Int. Ed.* **2006**, *45*, 6962−6984.

(6) Dissanayake, D.; Lunsford, J. The direct formation of H_2O_2 from H_2 and O_2 over colloidal palladium. *J. Catal.* **2003**, *214*, 113−120.

(7) Lari, G. M.; Puértolas, B.; Shahrokhi, M.; López, N.; Pérez-Ramírez, J. Hybrid palladium nanoparticles for direct hydrogen peroxide synthesis: the key role of the ligand. *Angew. Chem.* **2017**, *129*, 1801−1805.

(8) Liu, Q.; Bauer, J. C.; Schaak, R. E.; Lunsford, J. H. Direct synthesis of H_2O_2 from H_2 and O_2 over Pd−Pt/SiO_2 bimetallic catalysts in a H_2SO_4/ethanol system. *Appl. Catal., A* **2008**, *339*, 130−136.

(9) Han, Y.-F.; Zhong, Z.; Ramesh, K.; Chen, F.; Chen, L.; White, T.; Tay, Q.; Yaakub, S. N.; Wang, Z. Au promotional effects on the synthesis of H_2O_2 directly from H_2 and O_2 on supported Pd-Au alloy catalysts. *J. Phys. Chem. C* **2007**, *111*, 8410−8413.

(10) Wilson, N. M.; Flaherty, D. W. Mechanism for the direct synthesis of H_2O_2 on pd clusters: Heterolytic reaction pathways at the liquid−solid interface. *J. Am. Chem. Soc.* **2016**, *138*, 574−586.

(11) Tian, P.; Ouyang, L.; Xu, X.; Ao, C.; Xu, X.; Si, R.; Shen, X.; Lin, M.; Xu, J.; Han, Y.-F. The origin of palladium particle size effects in the direct synthesis of H_2O_2: Is smaller better? *J. Catal.* **2017**, *349*, 30−40.

(12) Edwards, J. K.; Hutchings, G. J. Palladium and gold–palladium catalysts for the direct synthesis of hydrogen peroxide. *Angew. Chem., Int. Ed.* **2008**, *47*, 9192–9198.

(13) F de L e Freitas, L.; Puértolas, B.; Zhang, J.; Wang, B.; Hoffman, A. S.; Bare, S. R.; Pérez-Ramírez, J.; Medlin, J. W.; Nikolla, E. Tunable catalytic performance of palladium nanoparticles for H_2O_2 direct synthesis via surface-bound ligands. *ACS Catal.* **2020**, *10*, 5202–5207.

(14) Liu, Q.; Lunsford, J. H. Controlling factors in the direct formation of H_2O_2 from H_2 and O_2 over a Pd/SiO_2 catalyst in ethanol. *Appl. Catal., A* **2006**, *314*, 94–100.

(15) Doronkin, D. E.; Wang, S.; Sharapa, D. I.; Deschner, B. J.; Sheppard, T. L.; Zimina, A.; Studt, F.; Dittmeyer, R.; Behrens, S.; Grunwaldt, J.-D. Dynamic structural changes of supported Pd, PdSn, and PdIn nanoparticles during continuous flow high pressure direct H_2O_2 synthesis. *Catal. Sci. Technol.* **2020**, *10*, 4726–4742.

(16) Selinsek, M.; Deschner, B. J.; Doronkin, D. E.; Sheppard, T. L.; Grunwaldt, J.-D.; Dittmeyer, R. Revealing the structure and mechanism of palladium during direct synthesis of hydrogen peroxide in continuous flow using operando spectroscopy. *ACS Catal.* **2018**, *8*, 2546–2557.

(17) Samanta, C. Direct synthesis of hydrogen peroxide from hydrogen and oxygen: An overview of recent developments in the process. *Appl. Catal., A* **2008**, *350*, 133–149.

(18) Guo, X.; Hoffman, A.; Yates, J. T., Jr. Adsorption kinetics and isotopic equilibration of oxygen adsorbed on the Pd (111) surface. *J. Chem. Phys.* **1989**, *90*, 5787–5792.

(19) Rose, M. K.; Borg, A.; Dunphy, J. C.; Mitsui, T.; Ogletree, D. F.; Salmeron, M. Chemisorption and dissociation of O_2 on Pd (111) studied by STM. *Surf. Sci.* **2003**, *547*, 162–170.

(20) Rose, M. K.; Borg, A.; Dunphy, J. C.; Mitsui, T.; Ogletree, D. F.; Salmeron, M. Chemisorption of atomic oxygen on Pd (111) studied by STM. *Surf. Sci.* **2004**, *561*, 69–78.

(21) Song, X.; Sun, K.; Hao, X.; Su, H.-Y.; Ma, X.; Xu, Y. Facet-Dependent of Catalytic Selectivity: The Case of H_2O_2 Direct Synthesis on Pd Surfaces. *J. Phys. Chem. C* **2019**, *123*, 26324.

(22) Kresse, G.; Hafner, J. Ab Initio Molecular Dynamics for Open-shell Transition Metals. *Phys. Rev. B: Condens. Matter Mater. Phys.* **1993**, *48*, 13115–13118.

(23) Kresse, G.; Hafner, J. Ab Initio Molecular-dynamics Simulation of the Liquid–metal–amorphous–semiconductor Transition in Germanium. *Phys. Rev. B: Condens. Matter Mater. Phys.* **1994**, *49*, 14251–14269.

(24) Kresse, G.; Furthmüller, J. Efficient Iterative Schemes for Ab Initio Total-energy Calculations Using a Plane-wave Basis Set. *Phys. Rev. B: Condens. Matter Mater. Phys.* **1996**, *54*, 11169–11186.

(25) Kresse, G.; Furthmüller, J. Efficiency of Ab-initio Total Energy Calculations for Metals and Semiconductors Using a Plane-wave Basis Set. *J. Comput. Mater. Sci.* **1996**, *6*, 15–50.

(26) We used VASP version 5.4.1.

(27) Blöchl, P. E. Projector Augmented-wave Method. *Phys. Rev. B: Condens. Matter Mater. Phys.* **1994**, *50*, 17953–17979.

(28) Kresse, G.; Joubert, D. From Ultrasoft Pseudopotentials to the Projector Augmented-wave Method. *Phys. Rev. B: Condens. Matter Mater. Phys.* **1999**, *59*, 1758–1775.

(29) Perdew, J. P.; Burke, K.; Ernzerhof, M. Generalized Gradient Approximation Made Simple. *Phys. Rev. Lett.* **1996**, *77*, 3865–3868.

(30) Grimme, S.; Antony, J.; Ehrlich, S.; Krieg, H. A Consistent and Accurate ab initio Parametrization of Density Functional Dispersion Correction (DFT-D) for the 94 Elements H-Pu. *J. Comput. Chem.* **2010**, *132*, 154104.

(31) Grimme, S.; Ehrlich, S.; Goerigk, L. Effect of the Damping Function in Dispersion Corrected Density Functional Theory. *J. Comput. Chem.* **2011**, *32*, 1456–1465.

(32) Schirber, J. E.; Morosin, B. Lattice constants of β–PdH_x and β–PdD_x with x near 1.0. *Phys. Rev. B: Solid State* **1975**, *12*, 117.

(33) Monkhorst, H. J.; Pack, J. D. Special points for Brillouin-zone integrations. *Phys. Rev. B: Solid State* **1976**, *13*, 5188–5192.

(34) Teschner, D.; Borsodi, J.; Wootsch, A.; Révay, Z.; Hävecker, M.; Knop-Gericke, A.; Jackson, S. D.; Schlögl, R. The roles of subsurface carbon and hydrogen in palladium-catalyzed alkyne hydrogenation. *Science* **2008**, *320*, 86–89.

(35) Hong, S.; Rahman, T. S. Adsorption and diffusion of hydrogen on Pd (211) and Pd (111): Results from first-principles electronic structure calculations. *Phys. Rev. B* **2007**, *75*, 155405.

(36) Mills, G.; Jónsson, H.; Schenter, G. K. Reversible Work Transition State Theory: Application to Dissociative Adsorption of Hydrogen. *Surf. Sci.* **1995**, *324*, 305–337.

(37) Henkelman, G.; Jónsson, H. Improved Tangent Estimate in the Nudged Elastic Band Method for Finding Minimum Energy Paths and Saddle Points. *J. Chem. Phys.* **2000**, *113*, 9978–9985.

(38) NIST Standard Reference Database.

(39) Rogal, J.; Reuter, K. Ab initio atomistic thermodynamics for surfaces: A primer. *Educational Notes RTO-EN-AVT-142*: Neuilly-sur-Seine 2007.

(40) McQuarrie, D. A.; Simon, J. D. *Molecular Thermodynamics*; University Science Books, 1999.

(41) Chorkendorff, I.; Niemantsverdriet, J. W. *Concepts of Modern Catalysis and Kinetics*; John Wiley & Sons, 2017.

(42) Virtanen, P.; Gommers, R.; Oliphant, T. E.; Haberland, M.; Reddy, T.; Cournapeau, D.; Burovski, E.; Peterson, P.; Weckesser, W.; Bright, J.; van der Walt, S. J.; Brett, M.; Wilson, J.; Millman, K. J.; Mayorov, N.; Nelson, A. R. J.; Jones, E.; Kern, R.; Larson, E.; Carey, C. J.; Polat, İ.; Feng, Y.; Moore, E. W.; VanderPlas, J.; Laxalde, D.; Perktold, J.; Cimrman, R.; Henriksen, I.; Quintero, E. A.; Harris, C. R.; Archibald, A. M.; Ribeiro, A. H.; Pedregosa, F.; van Mulbregt, P. SciPy 1.0 Contributors, SciPy 1.0: Fundamental Algorithms for Scientific Computing in Python. *Nat. Methods* **2020**, *17*, 261–272.

(43) Eyring, H. The activated complex and the absolute rate of chemical reactions. *Chem. Rev.* **1935**, *17*, 65–77.

(44) Stoltze, P. Surface Science as the Basis for the Understanding of the Catalytic Synthesis of Ammonia. *Phys. Scr.* **1987**, *36*, 824.

(45) Trinchero, A.; Hellman, A.; Grönbeck, H. Methane oxidation over Pd and Pt studied by DFT and kinetic modeling. *Surf. Sci.* **2013**, *616*, 206–213.

(46) Frieske, H.; Wicke, E. Magnetic susceptibility and equilibrium diagram of PdH_n. *Ber. Bunsen-Ges.* **1973**, *77*, 48–52.

(47) Johansson, M.; Skúlason, E.; Nielsen, G.; Murphy, S.; Nielsen, R. M.; Chorkendorff, I. Hydrogen adsorption on palladium and palladium hydride at 1 bar. *Surf. Sci.* **2010**, *604*, 718–729.

(48) Lundgren, E.; Kresse, G.; Klein, C.; Borg, M.; Andersen, J.; De Santis, M.; Gauthier, Y.; Konvicka, C.; Schmid, M.; Varga, P. Two-dimensional oxide on Pd (111). *Phys. Rev. Lett.* **2002**, *88*, 246103.

(49) Ketteler, G.; Ogletree, D. F.; Bluhm, H.; Liu, H.; Hebenstreit, E. L. D.; Salmeron, M. In situ spectroscopic study of the oxidation and reduction of Pd (111). *J. Am. Chem. Soc.* **2005**, *127*, 18269–18273.

(50) Jewell, L.; Davis, B. Review of absorption and adsorption in the hydrogen–palladium system. *Appl. Catal., A* **2006**, *310*, 1–15.

(51) Mitsui, T.; Rose, M. K.; Fomin, E.; Ogletree, D. F.; Salmeron, M. A scanning tunneling microscopy study of the reaction between hydrogen and oxygen to form water on Pd (111). *J. Chem. Phys.* **2002**, *117*, 5855–5858.

(52) Hammer, B. Special sites at noble and late transition metal catalysts. *Top. Catal.* **2006**, *37*, 3–16.

(53) Viñes, F.; Gomes, J. R. B.; Illas, F. Understanding the reactivity of metallic nanoparticles: beyond the extended surface model for catalysis. *Chem. Soc. Rev.* **2014**, *43*, 4922–4939.

(54) Landon, P.; Collier, P. J.; Carley, A. F.; Chadwick, D.; Papworth, A. J.; Burrows, A.; Kiely, C. J.; Hutchings, G. J. Direct synthesis of hydrogen peroxide from H_2 and O_2 using Pd and Au catalysts. *Phys. Chem. Chem. Phys.* **2003**, *5*, 1917–1923.

(55) Campbell, C. T. The Degree of Rate Control: A Powerful Tool for Catalysis Research. *ACS Catal.* **2017**, *7*, 2770.

(56) Kumar, G.; Van Cleve, T.; Park, J.; Van Duin, A.; Medlin, J. W.; Janik, M. J. Thermodynamics of alkanethiol self-assembled monolayer assembly on Pd surfaces. *Langmuir* **2018**, *34*, 6346–6357.

(57) Mark, L. O.; Zhu, C.; Medlin, J. W.; Heinz, H. Understanding the surface reactivity of ligand-protected metal nanoparticles for biomass upgrading. *ACS Catal.* **2020**, *10*, 5462−5474.

(58) Schoenbaum, C. A.; Schwartz, D. K.; Medlin, J. W. Controlling the surface environment of heterogeneous catalysts using self-assembled monolayers. *Acc. Chem. Res.* **2014**, *47*, 1438−1445.

(59) Lunsford, J. H. The direct formation of H_2O_2 from H_2 and O_2 over palladium catalysts. *J. Catal.* **2003**, *216*, 455−460.